Applied Physics Letters ARTICLE pubs.aip.org/aip/apl

Polarization-induced two-dimensional hole gases in N-polar AlGaN/GaN heterostructures

Cite as: Appl. Phys. Lett. **125**, 232101 (2024); doi: 10.1063/5.0241444
Submitted: 30 September 2024 · Accepted: 19 November 2024 ·
Published Online: 2 December 2024

Changkai Yu,[1,a)] Zexuan Zhang,[2] Debdeep Jena,[1,2,3] Huili Grace Xing,[1,2,3] and YongJin Cho[2,4,a)]

AFFILIATIONS

[1]Department of Materials Science and Engineering, Cornell University, Ithaca, New York 14853, USA
[2]School of Electrical and Computer Engineering, Cornell University, Ithaca, New York 14853, USA
[3]Kavli Institute at Cornell for Nanoscale Science, Cornell University, Ithaca, New York 14853, USA
[4]Paul-Drude-Institut für Festkörperelektronik, Leibniz-Institut im Forschungsverbund Berlin e.V., Hausvogteiplatz 5–7, 10117 Berlin, Germany

[a)]Authors to whom correspondence should be addressed: cy358@cornell.edu and cho@pdi-berlin.de

ABSTRACT

We report the observation of two-dimensional hole gases (2DHGs) in N-polar AlGaN/GaN heterostructures grown on single-crystal GaN substrates by plasma-assisted molecular beam epitaxy. A systematic study varying AlGaN barrier thickness is performed. The presence of 2DHGs is confirmed by persistent *p*-type conductivity and high hole mobility observed in temperature-dependent Hall-effect measurements down to 10 K, and the dependence of 2DHG density on the AlGaN barrier thickness indicates its polarization induced origin. 2DHG with a sheet density of 7.5×10^{12} cm^{-2} shows a relatively high hole mobility of 273 cm^2 V^{-1} s^{-1} at 10 K. Mobility model fit suggests that acoustic phonon scattering is the dominant scattering mechanism in the sub-room temperature region. This work indicates that the quality of N-polar 2DHGs is comparable to that of state-of-the-art metal-polar 2DHGs, contributing to a building block for potential high-quality N-polar *p*-channel devices.

Published under an exclusive license by AIP Publishing. https://doi.org/10.1063/5.0241444

03 December 2024 13:55:40

The recent years have witnessed tremendous research interest and progress made in the development of III-nitride semiconductor based *p*-channel transistors.[1–3] Combined with the well-developed *n*-channel transistors, such *p*-channel transistors would enable energy-efficient III-nitride based complementary technology for radio frequency (RF), power electronics, and other applications.[4–7] The development of *p*-channel transistors builds on the basis of two-dimensional hole gases (2DHGs) induced by the negative polarization sheet charge at AlGaN/GaN hetero-interfaces. High hole density and low sheet resistance can be achieved even without the use of chemical dopants. Recently, high-density hole gases with sheet density in excess of 4.5×10^{13} cm^{-2} have been demonstrated in undoped metal-polar GaN/AlN heterostructures.[8,9]

Concurrently, N-polar III-nitride heterostructures and devices have attracted significant attention. The inverted polarization field inherent in such heterostructures provides distinctive advantages and broad design space for electronic[10–13] and photonic[14,15] devices. However, *p*-channel devices on the N-polar platform have so far been lagging behind. By polarization engineering, substantial *p*-type conductivity has been achieved in compositionally graded N-polar AlGaN layers[16] and modulation-doped N-polar AlGaN/GaN superlattices.[17] In analogy to the two-dimensional electron gases in metal-polar AlGaN/GaN heterostructures, 2DHGs are expected to be induced in N-polar AlGaN/GaN heterostructures. Link *et al.*[18] reported the observation of 2DHG with a sheet hole density of 2×10^{13} cm^{-2} at room temperature in Mg-doped N-polar GaN/AlGaN/GaN heterostructure. Fandrich *et al.*[19] observed a 2DHG in N-polar AlGaN/GaN heterostructures grown by metalorganic vapor-phase epitaxy (MOVPE) with a sheet density of 1.6×10^{13} cm^{-2} and mobility of 52 cm^2 V^{-1} s^{-1} at room temperature. For N-polar AlGaN/GaN heterostructures, however, systematic impact of the AlGaN barrier thickness on the 2DHGs and characterizations of transport property at cryogenic temperatures—a critical signature of 2DHGs induced by polarization, have not been reported yet.

In this work, we report the effects of AlGaN barrier thickness on the formation of 2DHGs in N-polar AlGaN/GaN heterostructures grown on single-crystal GaN substrates by plasma-assisted molecular beam epitaxy (PAMBE). The hole density is seen to increase with the AlGaN barrier thickness. The temperature-dependent scattering mechanisms of the 2DHGs are also discussed using a mobility model fit.

N-polar AlGaN/GaN heterostructures were grown on semi-insulating Zn-doped N-polar single-crystal GaN substrates with a dislocation density of $\sim 5\times 10^6$ cm^{-2} produced by NGK Insulators, Ltd.

Published under an exclusive license by AIP Publishing

The root mean square (rms) roughness measured by an atomic force microscope (AFM) on a $20 \times 20\ \mu m^2$ area amounts to ~ 1.5 nm. The molecular beam epitaxy (MBE) growth of the heterostructures in this study was carried out in a Veeco GEN10 MBE system equipped with standard effusion cells for Ga, Al, and Mg, and a RF plasma source for active nitrogen species. During the MBE growth, the plasma source was operated with a RF power of 400 W and a N_2 gas flow rate of 1.25 sccm, resulting in a N-limited GaN growth rate of 315 nm h^{-1}. The growth front was monitored by *in situ* reflection high-energy electron diffraction (RHEED). For structural characterization, x-ray diffraction (XRD) measurements were carried out in a PANalytical Empyrean system using the Cu K $\alpha 1$ radiation (1.54056 Å). AFM using an Asylum Research Cypher ES setup was employed for surface morphology characterization of the samples. Electrical transport properties of the samples were characterized by temperature-dependent Hall-effect measurements under a magnetic field of 1.3 T in the van der Pauw geometry using soldered indium contacts.

Preceding the MBE growth, 5 mm × 5 mm GaN substrates were ultra-sonicated for 10 min each in acetone, methanol, and isopropanol in succession, loaded into the MBE system and outgassed at 200 °C to desorb water. *In situ* metal-assisted surface cleaning was carried out in the growth chamber to deoxidize the substrate surface. Similar metal-assisted deoxidation processes are routinely employed in the MBE growth of compound semiconductors including GaAs,[20–22] III-nitrides,[23–25] and Ga_2O_3.[26,27] 20 cycles of deoxidation were carried out at a thermocouple temperature of 760 °C, with each cycle consisting of 20 s of Ga deposition with a Ga beam equivalent pressure (BEP) of 6×10^{-7} Torr and 80–100 s of Ga desorption. Chamber pressure during this process was at $\sim 1 \times 10^{-9}$ Torr without the supply of N_2.

After the *in situ* surface cleaning, the substrate was cooled down to a thermocouple temperature of 670 °C for epitaxial growth. Figure 1(a) shows the schematic of the epitaxial structures in this study. A ~ 2 nm AlN insertion layer (IL) was grown first under N-rich conditions with an Al/N ratio of 0.8, followed by the deposition of a 300 nm thick GaN:Mg buffer layer under Ga-rich conditions. Here, the Mg doping with a density of 2.5×10^{18} cm^{-3} was intended to compensate for unintentional background donors in GaN, which typically lead to a free electron density of $\sim 2.5 \times 10^{17}$ cm^{-3} for N-polar GaN and can result in considerable *n*-type conductance for a thick GaN buffer layer. Room-temperature Hall-effect measurement revealed that the resulting GaN:Mg buffer layer exhibited a sheet resistance of ~ 600 k Ω/sq. The Mg shutter was then closed for the growth of a 5-nm-thick unintentionally doped (UID) GaN channel, and Al flux was provided for growth of the $Al_{0.26}Ga_{0.74}N$ barrier layer. After the MBE growth, the sample was cooled down immediately without the removal of excess Ga. A clear (3 × 3) surface reconstruction [Fig. 1(b)], the fingerprint of Ga adatom-on-adlayer structure on a N-polar GaN surface,[28] is observed, confirming the N-polarity of the AlGaN/GaN heterostructures.

The ultra-thin AlN IL served the purpose of capturing undesired donor dopants and suppressing impurity-induced conduction at the growth interface.[29] Large peak concentrations of silicon and oxygen (10^{18}–10^{19} cm^{-2}) were observed at the growth interface in secondary ion mass spectrometry (SIMS) measurement (not shown here), which would result in undesired *n*-type conduction at the growth interface. As shown in Fig. 1(c), with the ultra-thin AlN IL, a strong electric dipole bends the energy band and removes the conduction channel.[29] N-rich condition was used to promote the incorporation of impurities into the AlN IL, which would otherwise *float* on the growth front under Al-rich conditions and lead to *n*-type conductivity in GaN.[30] Moreover, it was recently reported that such AlN ILs also suppress the formation of surface pits and improve the surface morphology of N-polar GaN.[31]

03 December 2024 13:55:40

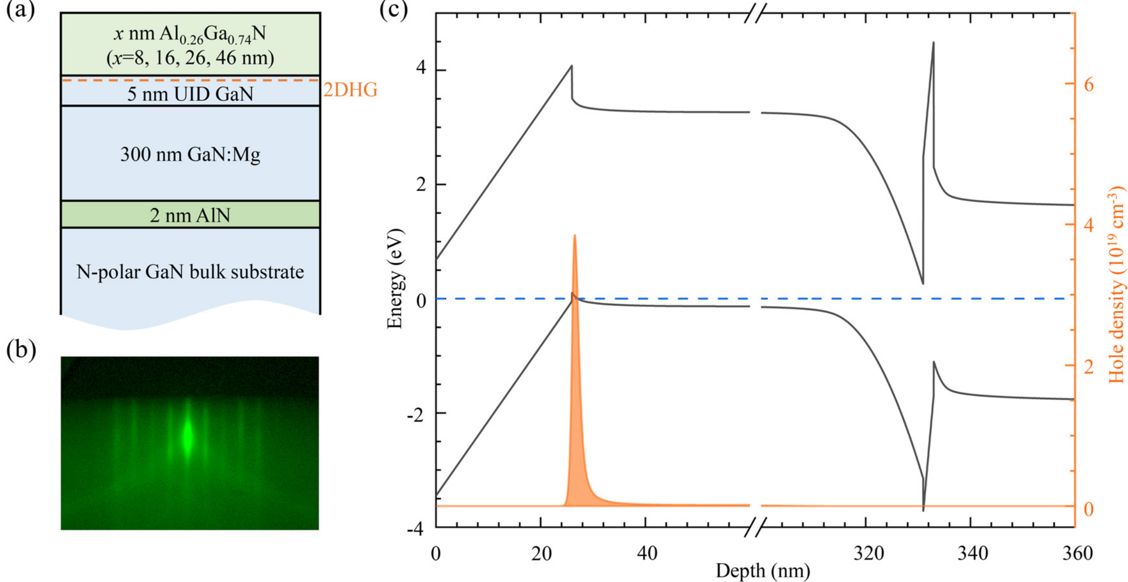

FIG. 1. (a) Schematic layer structure of N-polar AlGaN/GaN heterostructures. (b) RHEED pattern taken below 300 °C along the ⟨11$\bar{2}$0⟩ azimuth after growth. The (3 × 3) surface reconstruction confirms the N-polarity of the AlGaN/GaN heterostructures. (c) Calculated band diagram and hole density of N-polar AlGaN/GaN heterostructure with a 26 nm thick $Al_{0.26}Ga_{0.74}N$ barrier layer, where a surface barrier height of 3.45 eV is assumed for holes.

Published under an exclusive license by AIP Publishing

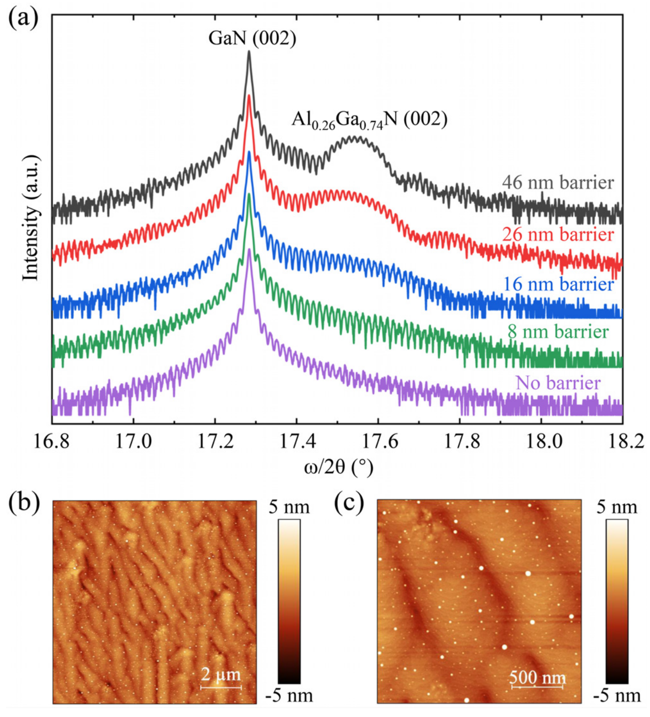

FIG. 2. (a) Symmetric XRD $\omega/2\theta$ scans of N-polar AlGaN/GaN heterostructures with different $Al_{0.26}Ga_{0.74}N$ barrier thickness. The "no barrier" sample lacks the $Al_{0.26}Ga_{0.74}N$ barrier on top. (b) $10 \times 10\ \mu m^2$ and (c) $2 \times 2\ \mu m^2$ AFM micrograph of the sample with 26 nm $Al_{0.26}Ga_{0.74}N$ barrier, serving as a representative. The rms roughness of the images (b) and (c) is 0.86 and 0.83 nm, respectively.

The structural abruptness of the heterostructures is witnessed by two sets of thickness fringes in symmetric XRD $\omega/2\theta$ scans [Fig. 2(a)]: the sparse ones arise from the top AlGaN barrier and the dense ones originate from the MBE-grown GaN and GaN:Mg layers. The appearance of the latter is due to the structural discontinuity with the underlying GaN substrate created by the ultra-thin AlN IL. Furthermore, the impact of the different $Al_{0.26}Ga_{0.74}N$ barrier thickness on the XRD scans is well resolved by the gradual change in the peak intensities [Fig. 2(a)].

The surface of the N-polar AlGaN/GaN heterostructures is characterized by fingerlike features with meandering atomic steps [Figs. 2(b) and 2(c)]. Such kinetically driven morphological instabilities are believed to result from pronounced Ehrlich–Schwöbel barrier at the atomic steps and the relatively low adatom mobility.[32] These features are often observed on the surface of MBE-grown N-polar nitrides.[33–35]

Now, we turn to the impact of the AlGaN barrier thickness on the transport properties of N-polar AlGaN/GaN heterostructures. First, it is noted that all the samples show *p*-type conduction at room temperature. The sheet resistance of the sample with 8 nm AlGaN barrier is seen to exponentially increase with decreasing temperature, implying the thermal deactivation of hole carriers [Fig. 3(a)] and therefore the conductivity originating from the GaN:Mg layer. On the other hand, the *p*-type conductivity persisted for the samples with thicker AlGaN barrier thicknesses throughout the measured temperature range, 10–290 K [Fig. 3(a)], accompanied by an increase in the hole density with the increasing AlGaN barrier thickness [Fig. 3(b)]. Although there exists a slight tendency of decreasing hole density with decreasing temperature [Fig. 3(b)], this behavior shows sharp contrasts to that of Mg-doped GaN.[8,16] Moreover, the measured mobility increases monotonically as temperature decreases [Fig. 3(c)], indicating characteristics of two-dimensional carrier gases dominated by

03 December 2024 13:55:40

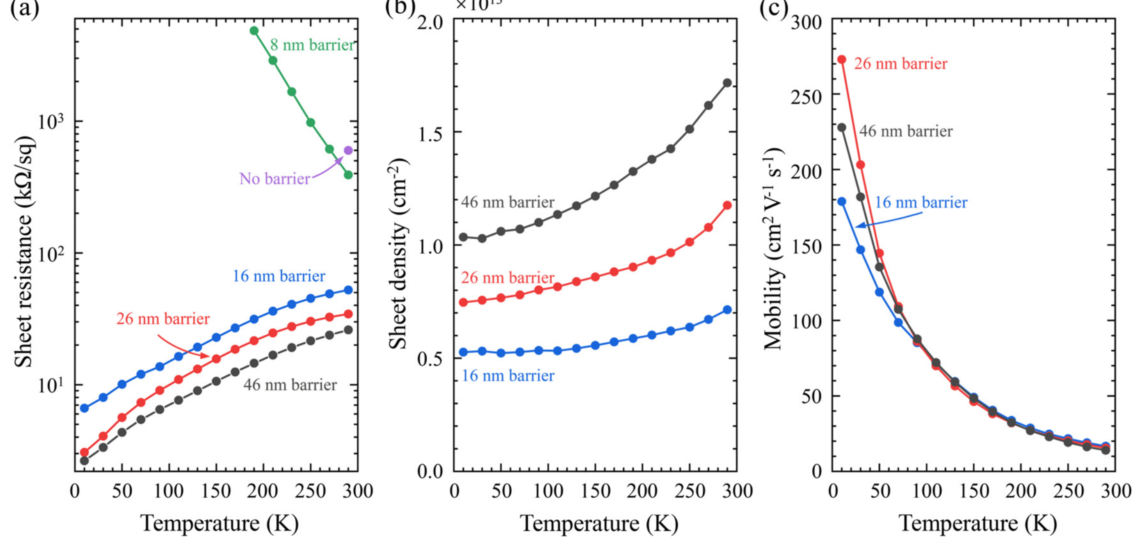

FIG. 3. (a) Sheet resistance, (b) sheet density, and (c) Hall mobility of N-polar AlGaN/GaN heterostructures with different $Al_{0.26}Ga_{0.74}N$ barrier thickness. Hall measurements on all AlGaN/GaN heterostructures confirmed hole-conducting channel.

Published under an exclusive license by AIP Publishing

intrinsic scattering mechanisms. The mobility measured for the 46, 26, and 16 nm barrier sample is 14, 15, and 17 $cm^2 V^{-1} s^{-1}$ at room temperature, respectively, and increases to 228, 273, and 179 $cm^2 V^{-1} s^{-1}$ at 10 K [Fig. 3(c)]. The highest hole mobility of 273 $cm^2 V^{-1} s^{-1}$ in the sample with 26 nm AlGaN barrier is comparable to that of the 2DHG in undoped GaN/AlN heterostructures grown on single-crystal AlN substrates.[9] As will be discussed later, these values are influenced by parallel conduction of holes in the buffer layer, which could lead to an underestimation of the 2DHG mobility, especially at room temperature. The sample with a thicker (46 nm) AlGaN barrier and thinner (16 nm) AlGaN barrier shows lower mobilities than the sample with 26 nm AlGaN barrier at low temperatures. The possible reasons for these observations are discussed below.

Using an analytical model similar to the one developed for metal-polar AlGaN/GaN two-dimensional electron gases (2DEGs),[36] the 2DHG density can be calculated as a function of thickness and Al composition of the AlGaN barrier. As shown in Fig. 4, there is a threshold thickness for the AlGaN barrier, above which 2DHGs can be induced. The exact value of the threshold thickness depends on the Al composition in the AlGaN layer, the surface barrier height, the valence band offset, and the polarization fields. The absence of a 2DHG in the 8 nm AlGaN barrier sample suggests that the threshold thickness is greater than 8 nm, and therefore, the surface barrier height for holes is larger than 2.4 eV. The valence band offset is assumed to be 0.11 eV between AlGaN and GaN in this calculation.

The measured sheet density in the samples at room temperature (open circles) and at 10 K (filled circles), together with the polarization sheet charge density, σ_{pol}, is shown in Fig. 4. The hole density increases with barrier thickness, in qualitative agreement with the theoretical prediction. It is worth noting that the measured hole densities are subject to the influence of non-negligible parallel conduction in the

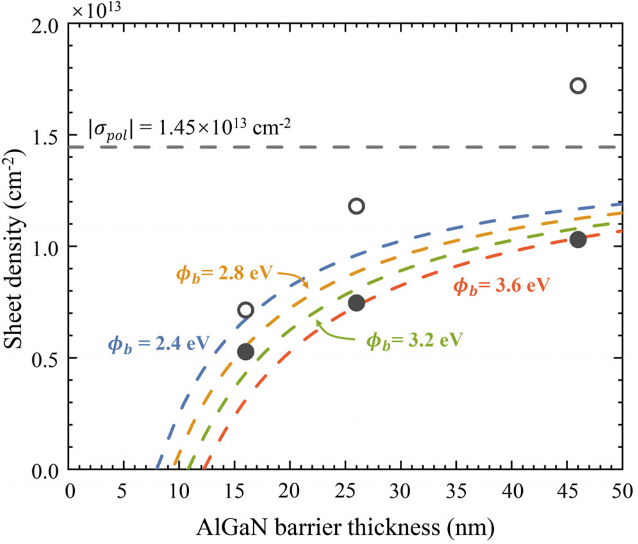

FIG. 4. Measured sheet hole density of N-polar AlGaN/GaN heterostructures with different $Al_{0.26}Ga_{0.74}N$ barrier thickness at room temperature (open circles) and 10 K (filled circles). The dashed lines indicate the polarization sheet charge density σ_{pol} (gray) at the AlGaN/GaN interface and 2DHG sheet densities (colored) calculated with different surface barrier heights for holes ϕ_b.

GaN:Mg buffer layer, as the measured sheet hole density of 1.7×10^{13} cm^{-2} at room temperature in the 46 nm barrier sample exceeds the polarization sheet charge density at the AlGaN/GaN hetero-interface. The influence of parallel conduction in the GaN:Mg buffer layer vanishes as temperature decreases [Fig. 3(a)]. However, the temperature dependence of the hole densities observed in the samples with 2DHGs cannot be fully explained by carrier freeze out. Otherwise, the hole densities would be sharply quenched with decreasing temperature due to the large activation energy ($\sim$200 meV) of Mg in GaN. This implies that there may be additional mechanisms contributing to the temperature dependence of 2DHG density observed in this work.

Similar phenomena have also been observed in MBE-grown undoped GaN/AlN heterostructures grown on AlN/sapphire templates[8] and single-crystal AlN substrates,[9] where no impurity dopants were introduced in the entire heterostructures. Zhang *et al.*[9] proposed temperature-dependent charge transfer between the 2DHG and surface states. The different magnitudes of decrease in hole density observed here indicate a complex charge balance between the 2DHG, surface states, and the buffer layer. Another possibility involves the simultaneous occupancy of both the heavy hole and light hole bands. In this case, parallel conduction of light holes in the 2DHG persists down to cryogenic temperatures, influencing Hall effect measurements. Given the presence of two *p*-type channels, the apparent sheet density in the low-field limit is expressed as $p_s = (p_1\mu_1 + p_2\mu_2)^2/(p_1\mu_1^2 + p_2\mu_2^2)$, where the subscripts denote the two channels. Since μ_1 and μ_2 are temperature-dependent, the measured hole density also varies with temperature. The underlying mechanism of the temperature dependence of hole density remains a subject of ongoing investigation.

The low field transport and mobility of 2DHG in GaN have been studied both theoretically[37,38] and experimentally.[8,9,39] It has been shown that phonon scattering limits mobility in the relatively high-temperature region, while low temperature mobility is determined by extrinsic scattering mechanisms such as dislocation, ionized impurity, alloy disorder, and interface roughness scattering. To gain insights into the scattering mechanisms in the 2DHGs, the temperature-dependent Hall mobility of the N-polar AlGaN/GaN with 26 nm AlGaN barrier is fitted with different scattering models (Fig. 5). Here, we follow the single-band approximation used in Ref. 9, in which the 2DHG is assumed to reside only in the heavy hole band and contribution from the light hole band is neglected. Phonon scattering mechanisms including acoustic deformation potential scattering, polar acoustic phonon (piezoelectric) scattering, and polar optical phonon scattering are considered. The mobility limited by extrinsic scattering mechanisms is presumed to be temperature-independent and is used as a "tuning parameter."[37] Contributions from different scattering mechanisms are combined by the Matthiessen's rule to give the overall mobility.

The mobility of a two-dimensional (2D) carrier system limited by acoustic deformation potential scattering calculated within the Fang–Howard approximation is given by Ref. 40,

$$\mu_{adp} \approx \frac{16e\rho v_s^2 \hbar^3}{3k_B T D_{ac}^2 m_h^2 b}, \tag{1}$$

where e is the elementary charge, $\rho = 6.15 \times 10^3$ kg m^{-3} is the mass density of GaN, $v_s = 7963$ m s^{-1} is the sound velocity in GaN, $\hbar$ is the reduced Planck's constant, k_B is the Boltzmann constant, T is temperature, $D_{ac} = 6.2$ eV is the valence band acoustic deformation

03 December 2024 13:55:40

Published under an exclusive license by AIP Publishing

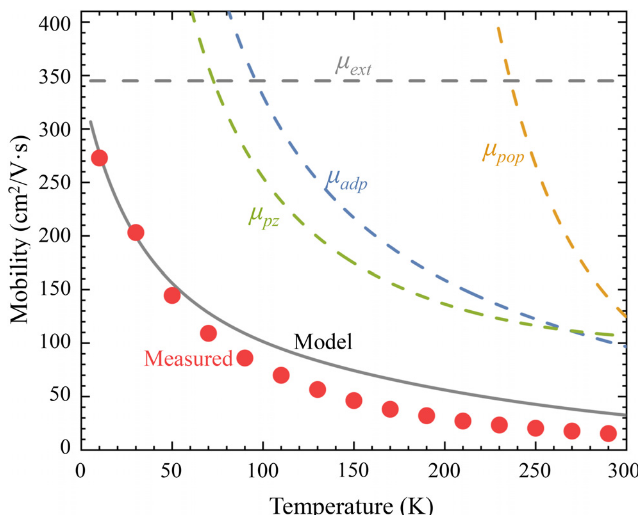

FIG. 5. Measured (red circles) and calculated (solid line) hole mobility as a function of temperature of N-polar AlGaN/GaN heterostructure with 26 nm thick $Al_{0.26}Ga_{0.74}N$ barrier. The dashed lines indicate the mobility limited by individual scattering mechanisms.

potential,[30] $m_h = 2m_0$ is the heavy hole effective mass,[37] and b is the variational parameter in Fang–Howard wavefunction of the 2D carrier system, given by $(33m_h e^2 p_s / 8\hbar^2 \varepsilon_0 \kappa_0)^{1/3}$. Here, p_s is the sheet hole density, ε_0 is the vacuum permittivity, and $\kappa_0 = 8.9$ is the static relative permittivity of GaN.

Due to the partially ionic nature of Ga-N bonds in GaN, the deformation of the lattice by phonons induces an extra electric field, which scatters the carriers. Depending on the nature of the perturbating phonons, such scattering can be categorized into polar acoustic phonon (piezoelectric) scattering and polar optical phonon scattering. The carrier mobility limited by piezoelectric scattering is given by Ref. 41,

$$\mu_{pz} \approx \frac{\pi^2 (\varepsilon_0 \kappa_0)^2 \rho v_s^2 \hbar^3}{2 e m_h^2 e_{pz}^2 k_B T} \Bigg/ \int_{\pi/2}^{3\pi/2} d\alpha \cos^2(\alpha)\, \mathcal{G}(-2k_F \cos\alpha), \tag{2}$$

where $e_{pz} = -0.551\ \mathrm{C/m^2}$ is the piezoelectric coefficient,[42] k_F is the in-plane Fermi vector of the 2D carrier gas, and $\mathcal{G}(x) = \pi(8b^3 + 9xb^2 + 3x^2 b)/8x(x+b)^3$. The other symbols have the same meanings as aforementioned. The 2DHG mobility limited by polar optical phonon scattering is given by Ref. 43,

$$\mu_{pop} \approx \frac{\varepsilon_0 \kappa^* k_0 \hbar^2}{2\pi e \omega_0 m_h^2 N G(k_0)} \left(1 + \frac{1 - e^{-y}}{y}\right), \tag{3}$$

where $1/\kappa^* = 1/\kappa_\infty - 1/\kappa_0$, $\kappa_\infty = 5.4$ is the high-frequency relative permittivity, $\hbar\omega_0 = 92$ meV is the optical phonon energy in GaN, $k_0 = (2m_h\omega_0/\hbar)^{1/2}$ is the carrier wave vector corresponding to optical phonon energy, $N = 1/(e^{\hbar\omega_0/k_B T} - 1)$ is the Bose–Einstein distribution function, $G(k_0) = k_0 \cdot \mathcal{G}(k_0)/\pi$ is the form factor, and $y = \pi\hbar^2 p_s / m_h k_B T$.

As shown in Fig. 5, scattering by acoustic phonons dominates the 2DHG mobility at high temperatures, consistent with previous works.[9,37] Based on our calculation, contributions from piezoelectric scattering and acoustic deformation potential scattering are comparable, different from the case of two-dimensional electron gases where piezoelectric scattering might be neglected.[44] A non-negligible discrepancy exists between our model and the experimental data (Fig. 5). In the following, we discuss potential mechanisms that might lead to such a discrepancy.

First, we discuss the influence of parallel conduction. In a two-carrier model, the measured Hall mobility is given by $\mu = (p_1\mu_1^2 + p_2\mu_2^2)/(p_1\mu_1 + p_2\mu_2)$ in the low-field limit. The presence of a low-mobility channel decreases the measured value, while the presence of a high-mobility channel increases the measured value. Despite the high sheet resistance of the GaN:Mg buffer layer, parallel conduction of holes with low mobility in the buffer layer could not be neglected and will result in a decrease in the measured mobility at relatively high temperatures. In addition, parallel conduction of light holes in the 2DHG, of which the mobility is expected to be higher than that of the heavy holes, could also influence the fitting process based on the single-band approximation. Specifically, the Hall effect measurement results could be an overestimation of the heavy hole mobility and consequently an underestimation of the heavy hole concentration, especially at cryogenic temperatures. Magnetoresistance measurements and quantitative mobility-spectrum analysis (QMSA)[45] could be performed to evaluate the impact of additional conduction channels. Moreover, inter-band scattering between the heavy hole and light hole band is not considered in this model.

We would also like to point out that the polarization coefficient of $-0.551\ \mathrm{C/m^2}$ used here is the so-called "proper" piezoelectric constant obtained by first-principle calculations.[42] A different value would lead to changes in the calculated piezoelectric scattering rate. Similarly, variations in the acoustic deformation potential yield different calculation results. However, the discrepancy cannot be resolved by varying these parameters in our calculation. Further investigation of the transport characteristics of low-density 2DHG in GaN is under way.

At low temperatures, the mobility of 2DHG is limited by extrinsic scattering mechanisms. The mobility measured at 10 K for the 46, 26, and 16 nm barrier sample is 228, 273, and 179 $\mathrm{cm^2\ V^{-1}\ s^{-1}}$, respectively. The non-monotonic change in 2DHG mobility can be explained by the density dependence of the extrinsic scattering mechanisms. As the 2DHG density decreases, the centroid of the 2DHG moves away from the AlGaN/GaN interface, leading to reduced alloy scattering and interface roughness scattering rates and enhanced mobility. However, with a further decrease in 2DHG density, mobility is expected to decrease due to the reduced electric screening and enhanced ionized impurity scattering and dislocation scattering.

In conclusion, we report the observation of 2DHGs in N-polar AlGaN/GaN heterostructures grown by PAMBE. The density of 2DHGs is tunable by changing the AlGaN barrier thickness. Hole mobility of 273 $\mathrm{cm^2\ V^{-1}\ s^{-1}}$ with a 2DHG density of $7.5 \times 10^{12}\ \mathrm{cm^{-2}}$ has been observed at 10 K. These results provide possibilities for the development of p-channel field-effect transistors and complementary technology based on N-polar GaN.

We would like to thank Dr. Vladimir Protasenko for the maintenance of the experimental apparatus. This work was supported by SUPREME, one of seven centers in JUMP 2.0, a Semiconductor Research Corporation (SRC) program sponsored by DARPA. This work made use of the Cornell Center for Materials Research shared instrumentation facility.

03 December 2024 13:55:40

Published under an exclusive license by AIP Publishing

AUTHOR DECLARATIONS

Conflict of Interest

The authors have no conflicts to disclose.

Author Contributions

Changkai Yu: Conceptualization (equal); Data curation (lead); Formal analysis (lead); Investigation (lead); Methodology (equal); Validation (equal); Writing – original draft (equal); Writing – review & editing (equal). **Zexuan Zhang:** Conceptualization (supporting); Formal analysis (supporting); Investigation (supporting); Methodology (supporting); Validation (supporting). **Debdeep Jena:** Conceptualization (supporting); Funding acquisition (lead); Investigation (supporting); Methodology (supporting); Project administration (supporting); Resources (supporting); Supervision (supporting); Validation (supporting); Writing – review & editing (equal). **Huili Grace Xing:** Conceptualization (supporting); Funding acquisition (lead); Investigation (supporting); Methodology (supporting); Project administration (supporting); Resources (lead); Supervision (lead); Validation (lead); Writing – review & editing (supporting). **YongJin Cho:** Conceptualization (equal); Investigation (equal); Methodology (lead); Project administration (equal); Resources (equal); Supervision (lead); Validation (lead); Writing – review & editing (lead).

DATA AVAILABILITY

The data that support the findings of this study are available from the corresponding authors upon reasonable request.

REFERENCES

[1]K. Nomoto, R. Chaudhuri, S. J. Bader, L. Li, A. Hickman, S. Huang, H. Lee, T. Maeda, H. W. Then, M. Radosavljevic, P. Fischer, A. Molnar, J. C. M. Hwang, H. G. Xing, and D. Jena, in *2020 IEEE International Electron Devices Meeting (IEDM)* (IEEE, 2020), pp. 8.3.1–8.3.4.
[2]L. Zhang, Z. Zheng, Y. Cheng, Y. H. Ng, S. Feng, W. Song, T. Chen, and K. J. Chen, in *2021 IEEE International Electron Devices Meeting (IEDM)* (IEEE, 2021), pp. 5.3.1–5.3.4.
[3]N. Chowdhury, Q. Xie, and T. Palacios, IEEE Electron Device Lett. **43**, 358 (2022).
[4]S. J. Bader, H. Lee, R. Chaudhuri, S. Huang, A. Hickman, A. Molnar, H. G. Xing, D. Jena, H. W. Then, N. Chowdhury, and T. Palacios, IEEE Trans. Electron Devices **67**, 4010 (2020).
[5]H. Amano, Y. Baines, E. Beam, M. Borga, T. Bouchet, P. R. Chalker, M. Charles, K. J. Chen, N. Chowdhury, R. Chu, C. D. Santi, M. M. D. Souza, S. Decoutere, L. D. Cioccio, B. Eckardt *et al.*, J. Phys. D: Appl. Phys. **51**, 163001 (2018).
[6]K. Hoo Teo, Y. Zhang, N. Chowdhury, S. Rakheja, R. Ma, Q. Xie, E. Yagyu, K. Yamanaka, K. Li, and T. Palacios, J. Appl. Phys. **130**, 160902 (2021).
[7]Z. Zheng, L. Zhang, W. Song, S. Feng, H. Xu, J. Sun, S. Yang, T. Chen, J. Wei, and K. J. Chen, Nat. Electron. **4**, 595 (2021).
[8]R. Chaudhuri, S. J. Bader, Z. Chen, D. A. Muller, H. G. Xing, and D. Jena, Science **365**, 1454 (2019).
[9]Z. Zhang, J. Encomendero, R. Chaudhuri, Y. Cho, V. Protasenko, K. Nomoto, K. Lee, M. Toita, H. G. Xing, and D. Jena, Appl. Phys. Lett. **119**, 162104 (2021b).
[10]W. Li, S. Sharmin, H. Ilatikhameneh, R. Rahman, Y. Lu, J. Wang, X. Yan, A. Seabaugh, G. Klimeck, D. Jena, and P. Fay, IEEE J. Explor. Solid-State Comput. Devices Circuits **1**, 28 (2015).
[11]Y. Cho, J. Encomendero, S.-T. Ho, H. G. Xing, and D. Jena, Appl. Phys. Lett. **117**, 143501 (2020a).
[12]S. Wienecke, B. Romanczyk, M. Guidry, H. Li, E. Ahmadi, K. Hestroffer, X. Zheng, S. Keller, and U. K. Mishra, IEEE Electron Device Lett. **38**, 359 (2017).
[13]B. Romanczyk, S. Wienecke, M. Guidry, H. Li, E. Ahmadi, X. Zheng, S. Keller, and U. K. Mishra, IEEE Trans. Electron Devices **65**, 45 (2018).
[14]J. Verma, J. Simon, V. Protasenko, T. Kosel, H. Grace Xing, and D. Jena, Appl. Phys. Lett. **99**, 171104 (2011).
[15]F. Akyol, D. N. Nath, S. Krishnamoorthy, P. S. Park, and S. Rajan, Appl. Phys. Lett. **100**, 111118 (2012).
[16]J. Simon, V. Protasenko, C. Lian, H. Xing, and D. Jena, Science **327**, 60 (2010).
[17]A. Krishna, A. Raj, N. Hatui, S. Keller, and U. K. Mishra, Appl. Phys. Lett. **115**, 172105 (2019).
[18]A. Link, O. Ambacher, I. Smorchkova, U. K. Mishra, J. S. Speck, and M. Stutzmann, *Silicon Carbide and Related Materials 2000*, Materials Science Forum Vol. 353 (Trans Tech Publications Ltd, 2001), pp. 787–790.
[19]M. Fandrich, T. Mehrtens, T. Aschenbrenner, T. Klein, M. Gebbe, S. Figge, C. Kruse, A. Rosenauer, and D. Hommel, J. Cryst. Growth **370**, 68 (2013).
[20]Y. Asaoka, J. Cryst. Growth **251**, 40 (2003).
[21]Z. R. Wasilewski, J.-M. Baribeau, M. Beaulieu, X. Wu, and G. I. Sproule, J. Vac. Sci. Technol. B **22**, 1534 (2004).
[22]T. Xia, Y.-J. Cho, M. Cotrufo, I. Agafonov, F. Van Otten, and A. Fiore, Semicond. Sci. Technol. **30**, 055009 (2015).
[23]D. F. Storm, D. S. Katzer, D. J. Meyer, and S. C. Binari, J. Appl. Phys. **112**, 013507 (2012).
[24]Y. Cho, C. S. Chang, K. Lee, M. Gong, K. Nomoto, M. Toita, L. J. Schowalter, D. A. Muller, D. Jena, and H. G. Xing, Appl. Phys. Lett. **116**, 172106 (2020b).
[25]Z. Zhang, Y. Hayashi, T. Tohei, A. Sakai, V. Protasenko, J. Singhal, H. Miyake, H. G. Xing, D. Jena, and Y. Cho, Sci. Adv. **8**, eabo6408 (2022).
[26]E. Ahmadi, O. S. Koksaldi, X. Zheng, T. Mates, Y. Oshima, U. K. Mishra, and J. S. Speck, Appl. Phys. Express **10**, 071101 (2017).
[27]T. Itoh, A. Mauze, Y. Zhang, and J. S. Speck, Appl. Phys. Lett. **117**, 152105 (2020).
[28]A. R. Smith, R. M. Feenstra, D. W. Greve, J. Neugebauer, and J. E. Northrup, Phys. Rev. Lett. **79**, 3934 (1997).
[29]Y. Cao, T. Zimmermann, H. Xing, and D. Jena, Appl. Phys. Lett. **96**, 042102 (2010).
[30]R. Chaudhuri, Z. Chen, D. A. Muller, H. G. Xing, and D. Jena, J. Appl. Phys. **130**, 025703 (2021).
[31]C. Wurm, E. Ahmadi, F. Wu, N. Hatui, S. Keller, J. Speck, and U. Mishra, Solid State Commun. **305**, 113763 (2020).
[32]N. A. K. Kaufmann, "Investigation of Indium-rich InGaN alloys and kinetic growth regime of GaN," Ph.D. thesis (EPFL, 2013).
[33]H. Turski, F. Krzyżewski, A. Feduniewicz-Żmuda, P. Wolny, M. Siekacz, G. Muziol, C. Cheze, K. Nowakowski-Szukudlarek, H. G. Xing, D. Jena, M. Załuska-Kotur, and C. Skierbiszewski, Appl. Surf. Sci. **484**, 771 (2019).
[34]K. Nomoto, H. G. Xing, D. Jena, and Y. Cho, Appl. Phys. Express **15**, 064004 (2022).
[35]Y. Cho, S. Sadofev, S. Fernández-Garrido, R. Calarco, H. Riechert, Z. Galazka, R. Uecker, and O. Brandt, Appl. Surf. Sci. **369**, 159 (2016).
[36]O. Ambacher, J. Smart, J. R. Shealy, N. G. Weimann, K. Chu, M. Murphy, W. J. Schaff, L. F. Eastman, R. Dimitrov, L. Wittmer, M. Stutzmann, W. Rieger, and J. Hilsenbeck, J. Appl. Phys. **85**, 3222 (1999).
[37]S. J. Bader, R. Chaudhuri, M. F. Schubert, H. W. Then, H. G. Xing, and D. Jena, Appl. Phys. Lett. **114**, 253501 (2019).
[38]C. Hamaguchi, J. Appl. Phys. **130**, 125701 (2021).
[39]C. Beckmann, J. Wieben, T. Zweipfennig, A. Kirchbrücher, J. Ehrler, R. Stamm, Z. Yang, H. Kalisch, and A. Vescan, J. Phys. D: Appl. Phys. **55**, 435102 (2022).
[40]J. H. Davies, *The Physics of Low-Dimensional Semiconductors: An Introduction* (Cambridge University Press, 1997).
[41]D. Jena, *Quantum Physics of Semiconductor Materials and Devices* (Oxford University Press, 2022).
[42]C. E. Dreyer, A. Janotti, C. G. Van de Walle, and D. Vanderbilt, Phys. Rev. X **6**, 021038 (2016).
[43]B. L. Gelmont, M. Shur, and M. Stroscio, J. Appl. Phys. **77**, 657 (1995).
[44]W. Knap, E. Borovitskaya, M. S. Shur, L. Hsu, W. Walukiewicz, E. Frayssinet, P. Lorenzini, N. Grandjean, C. Skierbiszewski, P. Prystawko, M. Leszczynski, and I. Grzegory, Appl. Phys. Lett. **80**, 1228 (2002).
[45]Z. Dziuba, Acta Phys. Pol., A **80**, 827 (1991).

03 December 2024 13:55:40

Published under an exclusive license by AIP Publishing